ACS APPLIED NANO MATERIALS

Open Access

This article is licensed under CC-BY 4.0

www.acsanm.org

Article

Enhanced Photocatalytic Activity of Titania Nanosheets via Morphology Control and Interface Engineering

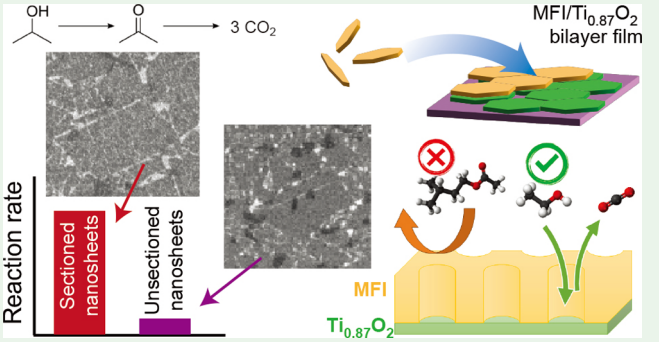
Ondřej Veselý, Nobuyuki Sakai,* and Takayoshi Sasaki

Cite This: *ACS Appl. Nano Mater.* 2026, 9, 20956–20966

Read Online

ACCESS | Metrics & More | Article Recommendations | Supporting Information

ABSTRACT: The photocatalytic oxidation of volatile organic compounds over titania nanosheets represents a promising strategy for efficient pollutant removal; however, the effects of nanosheet morphology and interface engineering on photocatalytic activity and selectivity remain insufficiently understood. In this study, titania nanosheets of a crystallographic thickness of 0.75 nm were assembled into molecularly thin monolayer films, and the photocatalytic oxidation of 2-propanol under UV irradiation was systematically examined using films with controlled nanosheet dimensions, different substrate electrical properties, and sectioned nanosheets. The initial reaction rate increased with increasing nanosheet size, whereas nanosheets with lateral dimensions of 3−6 μm exhibited the highest long-term photocatalytic activity. Increasing substrate resistivity enhanced the reaction rate but simultaneously brought about a shift in the product selectivity toward partially oxidized intermediates such as acetone. Further enhancement of the photocatalytic performance was achieved through nanosheet sectioning, which is attributed to the generation of edges exposing well-defined crystallographic facets. In addition, heterostructured bilayer films were designed by assembling a monolayer film of zeolite nanosheets onto a monolayer film of titania nanosheets, and their photocatalytic properties were examined. Although the intrinsic oxidation reactivity of the monolayer titania nanosheet film followed the order 2-propanol > ethanol > methanol, consistent with the relative stability of the intermediate radicals, deposition of a microporous MFI zeolite nanosheet overlayer decreased the overall conversion because of diffusional limitations, with the extent of conversion suppression depending on the kinetic diameter of the reactant. In particular, the conversion of larger alcohols was substantially suppressed, whereas that of methanol remained essentially unchanged, indicating that the MFI overlayer modulates the accessibility of reactants to the photocatalytically active surface. These findings demonstrate that both the activity and selectivity of titania nanosheet photocatalysts can be rationally tailored through control of the nanosheet morphology, substrate properties, and integration with a microporous overlayer.



KEYWORDS: *zeolite nanosheets, layered materials, exfoliation, nanofilm deposition, VOCs, photodecomposition*

INTRODUCTION

Titanium dioxide (TiO_2) is one of the most extensively studied semiconductor photocatalysts owing to its strong oxidative capability, excellent chemical stability, low toxicity, and natural abundance.[1−3] Upon light irradiation, TiO_2 generates photoexcited electron−hole pairs that initiate surface redox reactions, thereby enabling the oxidation of a wide variety of organic compounds.[4,5] Because these photocatalytic processes can proceed under ambient conditions using UV irradiation or even solar light, TiO_2 has attracted considerable attention for environmental remediation applications. Among various applications of TiO_2 photocatalysis, particular and intense attention has been paid to the degradation of volatile organic compounds (VOCs). VOCs constitute a diverse class of air pollutants commonly present in indoor and industrial environments, many of which are hazardous to human health, leading to secondary atmospheric pollution. TiO_2-based photocatalysis therefore offers a promising strategy for air purification through the efficient mineralization of VOCs into environmentally benign products such as CO_2 and H_2O.[2,6,7]

Beyond conventional bulk semiconductors, two-dimensional (2D) materials or nanosheets have emerged as an important class of photocatalysts, as their reduced dimensionality gives rise to unique physical and chemical properties.[8−10] In particular, metal oxide nanosheets such as $Ti_{1-\delta}O_2$ or $Ca_2Nb_3O_{10}$ are typically prepared through the exfoliation of layered precursors, yielding isolated single-crystalline sheets in which virtually all constituent atoms are exposed at the surface, in marked contrast

Received: October 4, 2026
Revised: October 9, 2026
Accepted: October 9, 2026
Published: October 17, 2026



ACS Publications

© 2026 The Authors. Published by American Chemical Society

Downloaded from pubs.acs.org/aanm6/article-pdf/9/44/20956/6889460/an6c04766.pdf by NATL INST FOR MATLS SCIENCE (NIMS) user on 07 November 2026

to bulk solids. Owing to their pronounced structural anisotropy, characterized by uniform thicknesses of only a few nanometers and lateral dimensions ranging from hundreds of nanometers to several micrometers, these nanosheets exhibit electronic structures substantially different from those of their bulk counterparts as a consequence of quantum confinement effects.[11−14] Such characteristics lead to modified band structures, anisotropic physicochemical properties, and enhanced redox potentials.[15−17] Although the photocatalytic properties of bulk and three-dimensional (3D) TiO_2 have been extensively studied, the application of titania nanosheets and related 2D materials to the degradation of VOCs remains comparatively underexplored.[18] At the same time, the electronic and interfacial properties of nanosheets can be readily tailored through assembly or molecular-level hybridization with other materials.[10,19−21] Furthermore, their colloidal suspensions enable facile processing and fabrication of diverse architectures and deposition onto a wide variety of substrates via solution-based processes, thereby offering considerable flexibility for the design of advanced photocatalytic systems.[17,22,23]

Previous studies on the photooxidative activity of titania nanosheets have largely focused on the photodecomposition of polycations and organic molecules confined within nanosheet galleries, as well as the photocatalytic mineralization of 2-propanol, a widely employed model VOC, into CO_2 under UV irradiation.[18,24] Although these studies clearly established the high photocatalytic activity of titania nanosheets, they have largely focused on the complete and nonselective oxidation of organic molecules to CO_2. Precise control over reaction selectivity is essential not only for suppressing the formation of undesirable intermediates but also for enabling partial oxidation toward value-added products and for achieving molecular size- or functionality-dependent reactivity. Consequently, the development of selective photocatalytic processes represents a critical step beyond simple pollutant degradation toward more sophisticated and tunable reaction systems.

Shape-selectivity, which arises from the confinement of reactant molecules within micropores of comparable dimensions, is a fundamental concept in heterogeneous catalysis.[25−28] Zeolites are among the most extensively studied and industrially utilized classes of microporous catalysts.[26,29] Although zeolites are generally recognized as 3D crystalline porous silicates, layered (2D) zeolite structures have been recently developed and further exfoliated into colloidal nanosheet dispersions.[30−34] These ultrathin zeolite nanosheets are particularly attractive because their 2D morphology facilitates intimate integration with other layered materials. In principle, their assembly with photocatalytically active titania nanosheets provides a pathway toward hybrid superstructures that combine the strong oxidative capability of titania with the intrinsic sieving effect of zeolitic micropores. Such architectures could provide a structural platform for regulating molecular access to reactive sites and thereby controlling photocatalytic reaction pathways.[35,36]

In the present study, we examine the photocatalytic activity and selectivity of monolayer films composed of titania nanosheets for the oxidation of 2-propanol under UV irradiation. Particular emphasis is placed on elucidating the effects of nanosheet size, morphology, and interactions with the underlying substrate on both photocatalytic activity and reaction pathways. In addition, we explore a strategy for controlling selectivity through the introduction of a microporous overlayer consisting of zeolite nanosheets designed to function as a molecular sieve. This hybrid architecture is intended to impose size-dependent accessibility to the photocatalytically active surface, thereby enabling the preferential oxidation of small VOC molecules while excluding larger organic species.

EXPERIMENTAL SECTION

Materials

TiO_2 (99.99%, Rare Metallic Co.), K_2CO_3 (99.9%, Rare Metallic Co.), Li_2CO_3 (99.99%, Rare Metallic Co.), MoO_3 (99.99%, Mitsuwa Chemicals), NaOH (99.2%, Lachner), aluminum sulfate hexadecahydrate (95%, Fluka analytical), H_2SO_4 (96%, Lachema), tetraethyl orthosilicate (TEOS, 98%, Sigma-Aldrich), tetrabutylammonium hydroxide (TBAOH, 10%, FUJIFILM Wako), dimethyl sulfoxide (DMSO, 99.0%, FUJIFILM Wako), 2-propanol (99.7%, FUJIFILM Wako), ethanol (99.5%, FUJIFILM Wako), and methanol (99.8%, FUJIFILM Wako) were used without further purification. Indium tin oxide (ITO, ∼200 nm thick, 2×10^{-4} Ω cm)-coated glass substrates with flat (R_a = 0.69 nm) and bumpy (R_a = 4.46 nm) surfaces were purchased from Kuramoto Co. and Furuuchi Chemical Co., respectively. Si (100) wafers (10 Ω cm) with a mirror-polished surface (R_a = 0.080 nm) and quartz glass substrates (R_a = 0.56 nm, 10^{18} Ω cm) were obtained from Furuuchi Chemical Co. Milli-Q filtered water was used throughout the experiments.

Preparation of $Ti_{0.87}O_2$ Nanosheet Suspensions

A colloidal aqueous suspension of $Ti_{0.87}O_2$ nanosheets was prepared following an established procedure.[37−39] First, a layered titanate, $K_{0.8}Ti_{1.73}Li_{0.27}O_4$, was synthesized by annealing a stoichiometric mixture of TiO_2, K_2CO_3, and Li_2CO_3 at 1000 °C for 20 h and subsequently ion-exchanged into a protonated form by the treatment with 1 M HCl solution at ambient temperature for 72 h. Subsequently, the obtained solid was dispersed in a solution of TBAOH ($TBA^+/H^+ = 1$, where H^+ represents the exchangeable protons in the protonic titanate) and exfoliated by continuous mechanical shaking at 180 rpm for 1 week or by intermittent manual shaking (ten strokes) two times a day for a period of 1 month into small- and medium-size nanosheets. The resulting suspension of $Ti_{0.87}O_2$ nanosheets was centrifuged at 10,000 rpm for 30 min. Then, the supernatant was decanted, and the sediment was dispersed in DMSO. The mass concentration of the nanosheets was determined by UV−vis spectroscopy from the absorbance at 270 nm using the molar extinction coefficient $\varepsilon = 1.12(1) \times 10^4$ mol^{-1} dm^3 cm^{-1} for micrometer-sized $Ti_{0.87}O_2$ nanosheets, and $1.33(1) \times 10^4$ mol^{-1} dm^3 cm^{-1} for sub-micrometer-sized $Ti_{0.87}O_2$ nanosheets, and the density of DMSO (ρ = 1.10 g cm^{-3}).[40]

The large titania nanosheets were derived from flux-grown titanate crystals.[41−43] A Pt crucible was loaded with the mixture of TiO_2, K_2CO_3, Li_2CO_3, and MoO_3 in a molar ratio of 1.73:1.67:0.13:1.27 and heated to 1200 °C for 10 h. After cooling down, the K_2MoO_4 flux melt was dissolved with water to recover the $K_{0.8}Ti_{1.73}Li_{0.27}O_4$ platelet crystals of 50−100 μm in size. Subsequently, 1 g of the $K_{0.8}Ti_{1.73}$-Li0.27O_4 crystals was treated with 100 mL of 1 M HCl under static conditions for 3 days while replacing the HCl solution with a fresh solution each day. The solid was collected by filtration and washed thoroughly with pure water to remove the residual acid.

Next, 0.2 g of the obtained crystals was gently mixed with 100 mL of 25.8 mM TBAOH aqueous solution ($TBA^+/H^+ = 1$), and the suspension was left standing overnight to promote extensive swelling. Afterward, the supernatant was decanted carefully, and an equal volume of DMSO was added, followed by gentle stirring. This process was repeated three times to remove as much of the residual water as possible. Finally, the suspension was shaken using a reciprocal shaker for 24 h to complete exfoliation.[43]

Preparation of MFI Suspension

Layered MFI zeolite was synthesized according to a published procedure using $[C_{22}H_{45}–N^+(CH_3)_2–C_6H_{12}–N^+(CH_3)_2–C_6H_{13}](Br^-)_2$, designated as C22-6-6 as a structure directing agent.[44−46] The synthesis gel was prepared by dissolving 37.37 g of NaOH in 840 g of water, adding

Downloaded from pubs.acs.org/aanm6/article-pdf/9/44/20956/6889546O/an6c04766.pdf by NATL INST FOR MATLS SCIENCE (NIMS) user on 07 November 2026

https://doi.org/10.1021/acsanm.6c04766
ACS Appl. Nano Mater. 2026, 9, 20956−20966

16.25 g of aluminum sulfate hexadecahydrate, 24.38 g of 96% H_2SO_4, and 324 g of tetraethyl orthosilicate (TEOS). Upon dissolution, 113 g of C22-6-6 was added, and the gel was transferred to a 2 L stainless-steel autoclave. The crystallization was carried out at 160 °C with rotation for 7 days. The product was recovered by filtration, washed with water, and dried at 60 °C. The as-synthesized zeolite was calcined at 350 °C for 10 h with a 10 h ramp.

Subsequently, 1 g of the calcined sample was dispersed in 20 mL of 10% TBAOH, stirred for 2 h, and centrifuged at 10,000 rpm for 30 min. The supernatant was discarded, and the sediment was mixed with 20 mL of water, shaken at 180 rpm for 24 h, and centrifuged at 10,000 rpm for 5 min. The supernatant was collected, and the sediment was shaken with water at 180 rpm. The process was repeated until the collected supernatant became clear (6−8 times). The collected supernatants from all cycles were combined and flocculated by acidification with 1 M HCl. The resulting solid was isolated by centrifugation and re-dispersed in 0.02 M TBAOH (ca. 0.5%).[32] The final suspension was centrifuged at 15,000 rpm for 30 min, and the sediment was re-dispersed in DMSO. The concentration of nanosheets in the suspension was estimated thermogravimetrically by heating an exact volume of the suspension in a Pt crucible at 85 °C to evaporate most of the solvent, followed by calcination at 450 °C for 6 h and then measuring the weight of the remaining solid.

Spin-Coating Deposition of Nanosheets

The cleaned substrate (1.5 cm × 1.5 cm) was anchored onto the sample holder of a spin coater (MS-B100, Mikasa) and covered with 60 μL of the DMSO-based suspension. $Ti_{0.87}O_2$ nanosheets were deposited from a 0.1% w/w suspension at 1650 rpm for 800 s.[47] MFI zeolite nanosheets were deposited from a 0.4% suspension by rotation at 1000 rpm for 10 s followed by 700 rpm for 800 s. The temperature was maintained at 26.5 ± 0.1 °C during spin-coating.

Photocatalytic Decomposition Test

The photocatalytic oxidation activity of the deposited films was examined by monitoring the decomposition of the reactant (2-propanol, ethanol, or methanol) under UV light.[18] A 500 W Xe short arc lamp (XEF-501SU, San-Ei Electric) was used as a light source. The incident light intensity was adjusted to a photon flux of 3.0×10^{16} cm^{-2} s^{-1} (λ = 200−300 nm) using a spectroradiometer (USR-45, Ushio). Samples with a total area of 22.5 cm^2 were arranged and enclosed in a 500 mL vessel equipped with a quartz glass lid, followed by an injection of approximately 700 ppmv of reagent through a septum. The vessel was stored in dark conditions until establishing an equilibrium between the reactant in the gas and adsorbed phases. Once a stable reactant concentration was confirmed, irradiation was started. Samples were analyzed using gas chromatography (GC-353B, GL Sciences Inc.). The apparent initial reaction rate constant, $k_{initial}$, for the oxidation of 2-propanol to acetone was obtained assuming the Langmuir−Hinshelwood reaction mechanism using the eqs 1 and 2, where c_{IPA} is the molar concentration of 2-propanol (mol L^{-1}) and t is time (for $t \leq 6$ h).[48−50]

$$k\, c_{IPA} = -\frac{dc_{IPA}}{dt} \quad (1)$$

$$\ln c_{IPA} = -k_{initial}\, t \quad (2)$$

Considering the overall low concentration of the reactants, competitive adsorption between 2-propanol and acetone was neglected. The experimental data, plotted on a semi-logarithmic scale, were fitted with a linear function, yielding the apparent rate constant as the slope of the fit function (2).

Characterization

X-ray diffraction (XRD) data were collected using a Rigaku Ultima IV powder diffractometer with monochromatized Cu Kα radiation (λ = 0.15406 nm). Scanning electron microscopy (SEM) images were obtained using a JEOL JSM-6010LA SEM at an acceleration voltage of 1 and 3 kV for deposited nanosheets and bulk samples, respectively. The average size of the nanosheets was obtained as an average width of 20 nanosheets for each sample. In-plane XRD measurements were performed using synchrotron X-ray radiation (λ = 0.11983(3) nm) at BL-6C, Photon Factory, High Energy Accelerator Research Organization (KEK). The X-rays were incident at an angle of 0.16° relative to the substrate surface, and the detector was revolved around the plane of the substrate at a scanning rate of 0.1°/min to measure the in-plane diffraction from the nanosheets. AFM imaging was carried out using a Hitachi AFM5200S scanning probe microscope equipped with a SI-DF20 cantilever in the tapping mode. Film roughness (R_a) was evaluated as an average of R_a values obtained over three separate spots on the sample.

RESULTS AND DISCUSSION

Size and Morphology of $Ti_{0.87}O_2$ Nanosheets

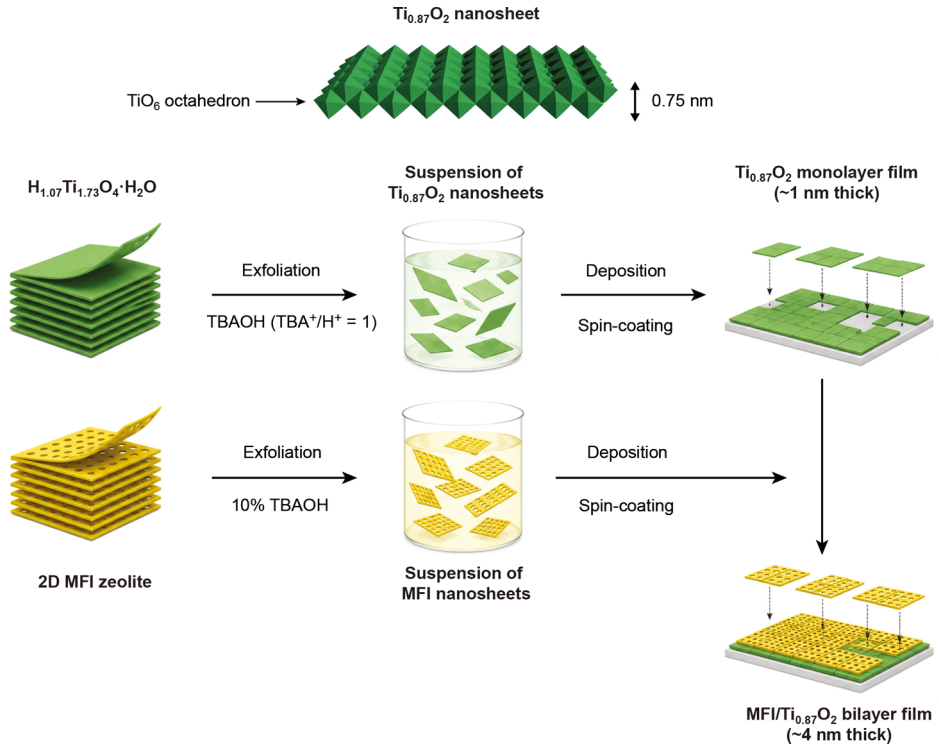
$Ti_{0.87}O_2$ nanosheets were prepared from a layered $H_{1.07}Ti_{1.73}O_4{\cdot}H_2O$ precursor via a soft-chemical exfoliation process according to previously established procedures (Scheme 1, Figure S1), yielding a suspension of 0.75 nm-thick unilamellar nanosheets.[39,47] The resulting nanosheets were deposited onto Si wafers by spin coating. SEM and AFM observations (Figures 1 and S2), together with in-plane XRD measurements (Figure S3), confirmed that the resulting molecularly thin films consisted of well-aligned $Ti_{0.87}O_2$ nanosheets with predominantly monolayer coverage, in good agreement with our previous reports.[47] As shown in Figure 1, the film surface contained only small gaps between adjacent nanosheets, observed as bright regions, together with occasional overlaps that appeared as darker contrast areas, while majority of the surface was covered by nanosheets in a monolayer. The lateral dimensions of the nanosheets were strongly influenced by the synthesis and exfoliation conditions. For convenience, the nanosheets were classified into three categories based on their average lateral dimensions: small, medium, and large. Continuous mechanical shaking during the exfoliation process produced nanosheets with an average lateral dimension (L) of 0.33 μm (small). In contrast, intermittent manual shaking yielded substantially larger nanosheets with an average lateral size of 4.6 μm (medium), whereas exfoliation of a precursor synthesized via a flux-assisted method under gentle conditions[41,43] afforded even larger nanosheets with an average lateral dimension of 12.8 μm (large). Films composed of small and medium nanosheets exhibited predominantly monolayer coverage of 86.4% and 83.8%, respectively (Table 1), thereby providing comparable illuminated and photocatalytically active surface areas. In contrast, the large nanosheets were less suitable for the formation of highly uniform monolayer films because their exceptionally large lateral dimensions hindered efficient tiling, resulting in a reduced monolayer coverage of 63.3%.

The molecularly thin monolayer films of $Ti_{0.87}O_2$ nanosheets deposited on Si wafers were evaluated in terms of the photocatalytic oxidation of 2-propanol under UV irradiation.[18] The initial reaction rate constants for the conversion of 2-propanol to acetone, the primary intermediate,[49,51] exhibited a clear dependence on nanosheet lateral size, increasing progressively with increasing nanosheet dimensions (Figures 2 and S4). Films composed of large nanosheets showed the highest initial reaction rates, whereas those consisting of small nanosheets exhibited the lowest photocatalytic activity. Previous studies have suggested that photogenerated electrons preferentially migrate toward energetically favorable edge states, while photogenerated holes remain distributed over the basal plane of the nanosheet.[52,53] Consequently, it is plausible that larger

Downloaded from pubs.acs.org/aanmf6/article-pdf/9/44/20956/6889546O/an6c04766.pdf by NATL INST FOR MATLS SCIENCE (NIMS) user on 07 November 2026

https://doi.org/10.1021/acsanm.6c04766
ACS Appl. Nano Mater. 2026, 9, 20956−20966

Scheme 1. Schematic Structure of $Ti_{0.87}O_2$ Nanosheets and the Fabrication Process of a Monolayer Film of $Ti_{0.87}O_2$ Nanosheets and a Bilayer Film of MFI/$Ti_{0.87}O_2$ Nanosheets



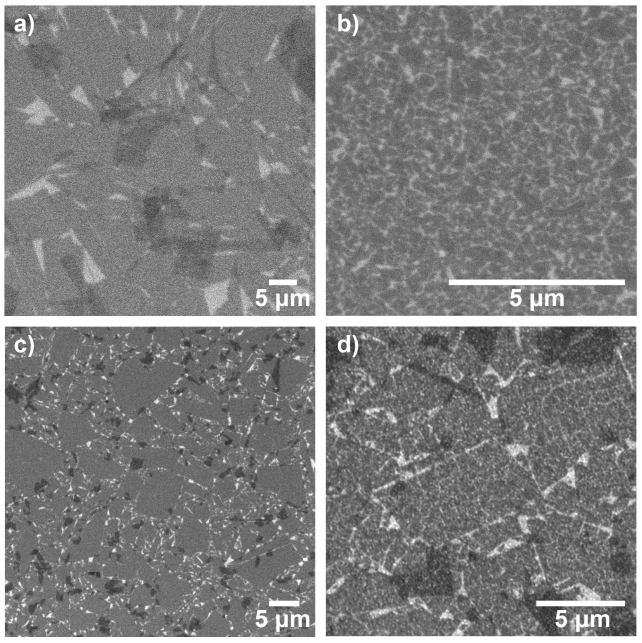


Figure 1. SEM images of (a) large, (b) small, and medium $Ti_{0.87}O_2$ nanosheets deposited on ITO substrates (c) without sectioning and (d) with sectioning.

nanosheets are expected to facilitate greater spatial separation of photogenerated charge carriers within an individual crystalline sheet, thereby suppressing electron−hole recombination and enhancing photocatalytic activity. However, the observed differences in photocatalytic activity may also be related to differences in the surface chemistry of the nanosheets, such as defect density or the type of facets exposed at the nanosheet edges, resulting from differences in the duration of the exfoliation treatment or the use of MoO_3 flux during the synthesis of the large nanosheets.

At longer irradiation times, however, pronounced differences in the photocatalytic behavior became evident among the samples. The large nanosheets exhibited a gradual deceleration of the reaction rate, reaching a maximum conversion of only 54.5% after 168 h of irradiation (Figure 2a), indicative of partial photocatalyst deactivation. These observations suggest that, although increasing nanosheet size enhances the initial reaction rate, an optimal nanosheet dimension exists for sustained long-term photocatalytic performance. While larger nanosheets may favor charge separation during the early stages of the reaction, their size and morphology may also influence adsorption behavior or increase susceptibility to mechanical, UV-induced, or reaction-induced surface modifications, thereby contributing to the observed deactivation.[54,55] Competitive adsorption between 2-propanol and the acetone intermediate may likewise contribute to the apparent loss of activity;[49,50] however, because similar behavior is not observed for the other more active samples, this is unlikely to be the dominant mechanism.

In contrast, the medium nanosheets displayed a sigmoidal conversion profile characterized by an initially delayed conversion of 2-propanol and the attainment of the maximum reaction rate only after approximately 48 h of irradiation (Figure 2a). Such behavior suggests the presence of an initially slow rate-determining step, commonly attributed to the dissociative adsorption of 2-propanol to form surface propoxy species prior to their subsequent oxidation into acetone.[49,51] Despite the initially suppressed activity, the medium nanosheets ultimately achieved a conversion of 82.7% after 168 h. The small nanosheets likewise exhibited indications of delayed activity; however, because of their overall lower reaction conversion, the existence of a

Downloaded from pubs.acs.org/aanm6/article-pdf/9/44/20956/6889460/an6c04766.pdf by NATL INST FOR MATLS SCIENCE (NIMS) user on 07 November 2026

https://doi.org/10.1021/acsanm.6c04766
ACS Appl. Nano Mater. 2026, 9, 20956–20966

Table 1. Lateral Dimensions of the Different Titania Nanosheets and the Surface Coverage and Roughness of Their Corresponding Monolayer Films

sample	L (μm)[a]	uncovered (%)[a]	monolayer (%)[a]	overlaps (%)[a]	R_a (nm)[b]
large	12.8 ± 4.0	11.5	63.3	25.1	0.53 ± 0.23
medium	4.6 ± 1.8	8.1	83.8	8.1	0.48 ± 0.17
small	0.33 ± 0.10	13.6	86.4	<1	0.50 ± 0.23

[a]Determined by SEM imaging of samples deposited on ITO substrates. [b]Determined by AFM imaging of samples deposited on Si substrates.

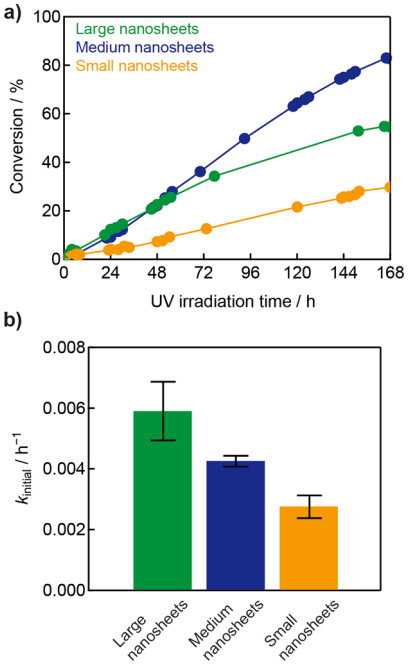


Figure 2. (a) Time course of photocatalytic conversion of 2-propanol over $Ti_{0.87}O_2$ nanosheet films with different lateral nanosheet dimensions under UV irradiation and (b) the corresponding initial reaction rate constants. Si substrates were used.

similarly adsorption-limited initial stage could neither be conclusively confirmed nor excluded.

Influence of the Substrate/Support

Monolayer films of $Ti_{0.87}O_2$ nanosheets can be fabricated on a wide variety of flat substrates, thereby enabling a systematic investigation of substrate effects on photocatalytic performance. The medium nanosheets were deposited onto three substrates with markedly different electrical resistivities: flat ITO-coated glass, Si, and quartz glass, with bulk resistivities of 2×10^{-4}, 10, and 10^{18} Ω cm, respectively, yielding monolayer films of comparable quality (Tables S1,S2 and Figure S5). Photocatalytic measurements revealed that the initial reaction rate increased with increasing substrate resistivity (Figure 3a,b). This correlation demonstrates that the electrical properties of the substrate influence the photocatalytic performance of the nanosheet films. For highly conductive substrates, photogenerated electrons may be readily injected from the nanosheets into the substrate, where they can migrate efficiently across the sample. Such electron transport increases the probability of recombination with photogenerated holes remaining in the nanosheets, thereby suppressing the photocatalytic reaction rate and lowering the overall conversion. This interpretation is consistent with the band alignment of the $Ti_{0.87}O_2$ nanosheets and the respective substrates (Figure S6).[11,56−58] The

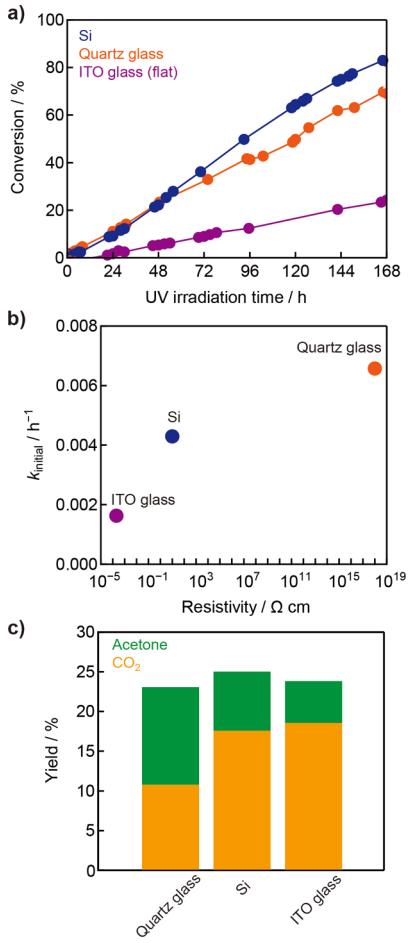


Figure 3. (a) Time course of photocatalytic conversion of 2-propanol over medium $Ti_{0.87}O_2$ nanosheet films deposited on different substrates and (b) initial reaction rate constants for the photocatalytic oxidation of 2-propanol plotted as a function of substrate resistivity. (c) Yields of acetone and CO_2 at approximately a 25% conversion of 2-propanol.

conduction band of ITO lies at a lower energy level than that of the $Ti_{0.87}O_2$ nanosheets, suggesting that electron transfer from the nanosheets to the ITO substrate is energetically favorable.[59,60] In contrast, Si and quartz glass substrates possess conduction bands located at comparable or higher energy levels relative to the $Ti_{0.87}O_2$ nanosheets, rendering electron transfer energetically less favorable. However, the photocatalytic performance may also be influenced by other interfacial factors, such as the substrate work function and surface electronic structure, which can affect charge transfer between the nanosheets and the substrates. Because the present results do not allow these factors to be independently evaluated or their relative contributions to be determined, the observed dependence

Downloaded from pubs.acs.org/aanm6/article-pdf/9/44/20956/6889460/an6c04766.pdf by NATL INST FOR MATLS SCIENCE (NIMS) user on 07 November 2026

https://doi.org/10.1021/acsanm.6c04766
ACS Appl. Nano Mater. 2026, 9, 20956−20966

of photocatalytic activity on substrate resistivity cannot be attributed solely to substrate-mediated electron transfer. Nevertheless, the proposed electron-transfer mechanism provides a plausible explanation for the observed trend and is consistent with the band alignment of the $Ti_{0.87}O_2$ nanosheets and the respective substrates.

Despite this overall trend, the 2-propanol conversion achieved over the nanosheet film deposited on Si eventually exceeded that observed for the quartz glass-supported sample, indicating that the substrate affects not only the initial reaction kinetics but also the longer-term photocatalytic performance. To further evaluate the influence of the substrate on product selectivity, yields of products were compared at approximately a 25% conversion of 2-propanol. The acetone yields, 5.5% for ITO, 7.7% for Si, and 12.5% for quartz glass, increased progressively with increasing substrate resistivity (Figures 3c and S7). These results suggest that, although substrate-dependent charge separation efficiency is the dominant factor governing the initial oxidation step from 2-propanol to acetone, it exerts less influence on the subsequent oxidation of acetone to CO_2, a process involving not only photogenerated holes but also reactive oxygen species.[48,50] Consequently, acetone accumulates to a greater extent over the quartz-glass-supported photocatalyst, and longer irradiation times are required for complete oxidation, despite the relatively rapid initial conversion of 2-propanol (Figure S7a). The accumulation of intermediate species such as acetone is generally undesirable in VOC abatement because such intermediates may present greater health risks than the parent compounds themselves.[36] Nevertheless, this type of photocatalytic behavior may be advantageous for partial oxidation processes aimed at the selective synthesis of value-added chemicals.[61,62]

Activity Enhancement by Sectioning

The size and morphology of $Ti_{0.87}O_2$ nanosheets can be tailored not only through the exfoliation process but also via post-deposition structural modification. We have previously demonstrated that sectioning of nanosheets along their principal crystallographic axes can be induced by tensile stress applied laterally to the nanosheets upon contact with a bumpy substrate surface.[40] Based on this approach, the medium $Ti_{0.87}O_2$ nanosheets were deposited onto both flat and bumpy ITO substrates. While the deposition onto flat ITO preserved the nanosheets in their original morphology, spin coating onto the bumpy ITO surface induced pronounced sectioning, as confirmed by SEM observations (Figure 1c,d). The SEM image shows white lines extending across the nanosheets, which are attributed to cracks formed within the nanosheets (Figure 1d). These cracks are predominantly orthogonal to one another. Considering the two-dimensional rectangular lattice structure of the $Ti_{0.87}O_2$ nanosheets, the orthogonal arrangement of the cracks suggests that the nanosheets are sectioned along the [100] and [001] crystallographic axes. Therefore, the sectioning produces well-defined edges preferentially aligned along these crystallographic directions. In contrast, the edges of the unsectioned nanosheets are generated primarily through mechanical fragmentation during agitation in the exfoliation process and therefore possess largely random crystallographic orientations.

Photocatalytic experiments revealed that the sectioned nanosheets exhibited markedly enhanced activity relative to that of the unsectioned samples. Sectioning increased the 2-propanol conversion after 168 h from 24.2% to 96.1% (Figure 4a), accompanied by an approximately 8-fold increase in the initial

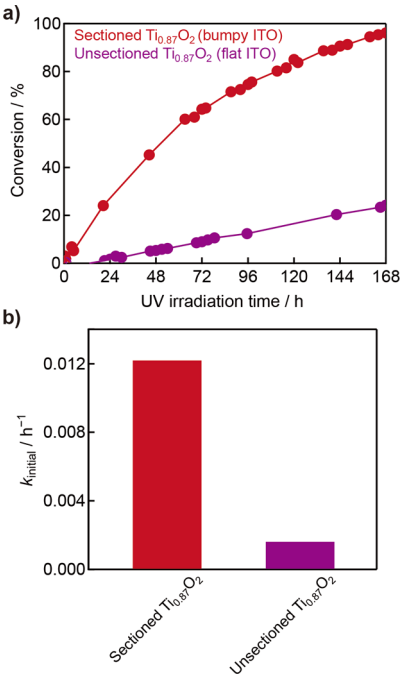


Figure 4. (a) Time course of photocatalytic conversion of 2-propanol over sectioned and unsectioned medium $Ti_{0.87}O_2$ nanosheets deposited on bumpy and flat ITO glass substrates, respectively, and (b) the corresponding initial reaction rate constants for 2-propanol photooxidation.

reaction rate (Figure 4b). Notably, the sectioned medium $Ti_{0.87}O_2$ nanosheets exhibited higher photocatalytic activity than both the large nanosheets supported on Si and the medium nanosheets supported on quartz glass (Figure 2b and Figure 3b). These samples were selected as reference points because they exhibited the highest initial reaction rates in the nanosheet size-dependent and substrate-dependent experiments. Although these comparisons involve differences in both nanosheet size and substrate, they provide useful benchmarks for evaluating the activity of the sectioned nanosheets within the scope of the present study. The substrate dependence experiments showed that the use of ITO suppressed the photocatalytic activity compared with Si and quartz glass. Nevertheless, the sectioned medium nanosheets supported on ITO exhibited higher activity than both reference samples. This suggests that using a nonflat Si or quartz glass substrate instead of ITO for nanosheet sectioning could lead to an even higher photocatalytic activity.

The edges of the unsectioned nanosheets are likely passivated through prolonged exposure to the aqueous TBAOH solution during the exfoliation process. Indeed, monolayer films prepared from nanosheet suspensions stored for extended periods exhibited photocatalytic activities essentially identical to those of films prepared from freshly exfoliated suspensions (Figure S8a). In contrast, the enhanced activity of the sectioned nanosheets may initially be attributed to the generation of newly exposed edges during the sectioning process. To examine this possibility, films composed of sectioned nanosheets were intentionally aged by immersion in an aqueous TBAOH solution. However, even after this treatment, the aged films retained their high photocatalytic activity (Figure S8b), suggesting that the enhanced performance does not simply originate from the freshness of the exposed edges. Furthermore, the small $Ti_{0.87}O_2$ nanosheets, which exhibit a lateral size comparable to that of the sectioned

Downloaded from pubs.acs.org/aanmf6/article-pdf/9/44/20956/6889460/an6c04766.pdf by NATL INST FOR MATLS SCIENCE (NIMS) user on 07 November 2026

https://doi.org/10.1021/acsanm.6c04766
ACS Appl. Nano Mater. 2026, 9, 20956–20966

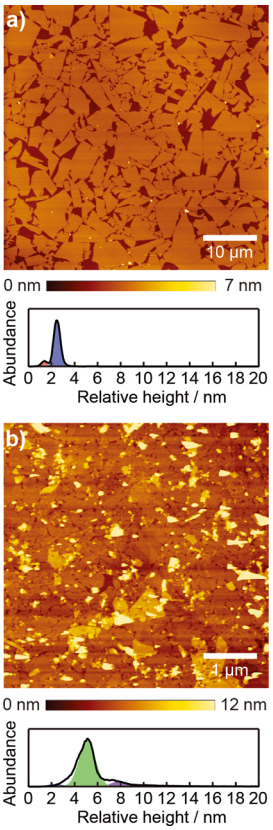


Figure 5. AFM images of (a) a monolayer film of medium $Ti_{0.87}O_2$ nanosheets and (b) a $Ti_{0.87}O_2$ nanosheet film covered with a monolayer of MFI zeolite nanosheets deposited by spin coating, together with the corresponding height histograms deconvoluted into exposed substrate (red), monolayer $Ti_{0.87}O_2$ nanosheets (blue), monolayer MFI nanosheets on top of $Ti_{0.87}O_2$ nanosheets (green), and overlapped MFI nanosheets (purple).

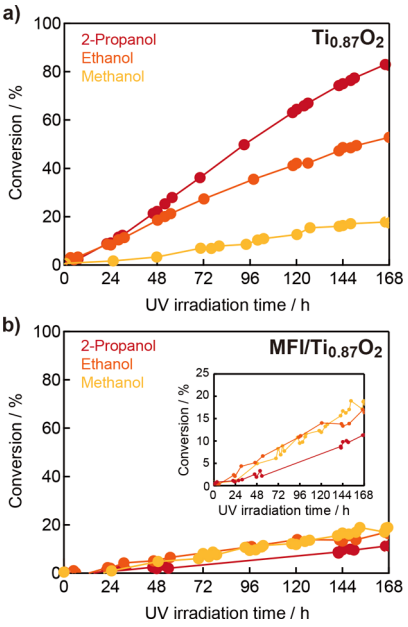


Figure 6. Time course of photocatalytic conversion of 2-propanol, ethanol, and methanol over (a) a monolayer film of medium $Ti_{0.87}O_2$ nanosheets and (b) a bilayer film consisting of an MFI nanosheet monolayer deposited on top of a $Ti_{0.87}O_2$ nanosheet monolayer. The inset is an enlarged view of the *y*-axis range in panel b. Si substrates were used.

nanosheets, showed lower photocatalytic activity than the sectioned nanosheets (Figure S8), indicating that the enhanced activity of the sectioned nanosheets is not merely a result of their increased edge or vacancy density per unit sample area. The native edges of titania nanosheets have previously been reported to serve as preferential sites for the photocatalytic reductive deposition of metals such as Ag and Cu.[52] It has also been reported that the photocatalytic activity of bulk anatase- and rutile-type TiO_2 depend on the exposed crystallographic facets.[63,64] It is therefore plausible that the well-defined crystallographic facets generated through nanosheet sectioning play a decisive role in enhancing the photocatalytic activity. However, while the edges generated through nanosheet sectioning may enhance the photocatalytic oxidation activity, additional parameters including the formation of specific defects or vacancies or even differences in light scattering from the bumpy ITO substrate may influence the reaction rate.[8,14,60,65] A further study is needed to verify the mechanism.

Zeolite-Imposed Reactant Accessibility

We further examined the control of photocatalytic selectivity through the assembly of a zeolite nanosheet overlayer on $Ti_{0.87}O_2$ nanosheets. A layered ZSM-5 zeolite possessing the MFI topology, characterized by interconnected 10-membered-ring channels with pore dimensions of 5.1 Å × 5.5 Å and 5.3 Å × 5.6 Å, was synthesized (Figure S9) and subsequently exfoliated according to the established procedure developed by Roth and co-workers.[32] Spin coating of the exfoliated MFI nanosheets produced a compact film exhibiting 76.3% monolayer coverage, while the measured nanosheet thickness of 2.8 nm was consistent with previously reported values (Figure S10). The remaining surface area consisted primarily of narrow gaps between adjacent nanosheets, locally overlapped regions, and small semicircular particles originating from non-exfoliated MFI zeolite fragments. Based on these nanosheets, a bilayer hybrid photocatalyst was fabricated by depositing a monolayer film of MFI nanosheets onto a monolayer film of $Ti_{0.87}O_2$ nanosheets. The presence of both $Ti_{0.87}O_2$ and MFI nanosheets in the bilayer film was confirmed by in-plane XRD measurements, which exhibited characteristic reflections attributable to each component (Figure S3). The monolayer film of $Ti_{0.87}O_2$ nanosheets exhibited an average thickness of 1.1 nm and a monolayer coverage of 83.8%, whereas the bilayer film showed additional layers with a thickness of 2.8 nm corresponding to the MFI nanosheets, thereby indicating the successful formation of the bilayer architecture (Figure 5a,b).

The photocatalytic performance of the monolayer and bilayer photocatalysts was evaluated using three alcohol reactants of different molecular sizes and structures: methanol, ethanol, and 2-propanol. Over the monolayer film of $Ti_{0.87}O_2$ nanosheets, the observed conversion strongly depended on both the molecular size and the degree of substitution of the reactants, increasing from 17.4% for methanol to 52.9% for ethanol and further to 82.7% for 2-propanol (Figure 6a). This trend can be rationalized in terms of the relative stability of the intermediate α-hydroxyalkyl radicals generated through hydrogen abstraction from the α-carbon during the oxidation process. The primary $^{\bullet}CH_2OH$ radical derived from methanol is the least stable, followed by the secondary $^{\bullet}CH(CH_3)OH$ radical formed from ethanol, whereas the tertiary $^{\bullet}C(CH_3)_2OH$ radical generated

Downloaded from pubs.acs.org/aanm6/article-pdf/9/44/20956/6889546O/an6c04766.pdf by NATL INST FOR MATLS SCIENCE (NIMS) user on 07 November 2026

https://doi.org/10.1021/acsanm.6c04766
ACS Appl. Nano Mater. 2026, 9, 20956–20966

from 2-propanol is the most stable, leading to progressively enhanced reaction rate across the series.[66−68] This is supported by the experimental observations where methanol exhibits the lowest initial reaction rate over $Ti_{0.87}O_2$, followed by ethanol and 2-propanol (Figure S11).

Deposition of the MFI overlayer resulted in a substantial decrease in the conversion of the larger alcohols, reducing the reaction conversion from 82.7% to 11.2% for 2-propanol and from 52.9% to 16.3% for ethanol (Figure 6b). In contrast, the methanol conversion over the MFI/$Ti_{0.87}O_2$ bilayer photocatalyst remained essentially unchanged, exhibiting only a marginal increase from 17.4% to 18.9%, which falls within the experimental error. If the decrease in the reaction conversion of 2-propanol and ethanol were simply due to a reduction in the exposed surface area of the $Ti_{0.87}O_2$ nanosheets caused by the MFI overlayer, the reaction conversion of methanol should also decrease by a similar proportion. However, this is not the case. Therefore, it is plausible that, in addition to reacting on the exposed $Ti_{0.87}O_2$ nanosheet surface, a fraction of the alcohol molecules reaches the $Ti_{0.87}O_2$ surface through the micropores of the MFI nanosheets and undergoes oxidation there, contributing to the observed differences in reaction conversion. Based on the AFM observation of the monolayer film of MFI nanosheets (Figure S10), we estimated that 4.6% of the $Ti_{0.87}O_2$ nanosheet surface remains exposed and uncovered by the MFI nanosheets in the bilayer film. Using this value and the reaction rates obtained for the monolayer film of $Ti_{0.87}O_2$ nanosheets, the contributions of the exposed $Ti_{0.87}O_2$ nanosheets to the overall reaction conversion were estimated to be 3.8% for 2-propanol, 2.4% for ethanol, and 0.8% for methanol. Accordingly, the conversions attributable to the $Ti_{0.87}O_2$ nanosheets covered by the MFI nanosheets were estimated by subtracting these contributions from the overall conversions observed for the MFI/$Ti_{0.87}O_2$ bilayer film, yielding 7.4% for 2-propanol, 13.9% for ethanol, and 18.1% for methanol. Comparison with the corresponding reaction conversions of the monolayer film of $Ti_{0.87}O_2$ nanosheets indicates that MFI overlayer coverage has little effect on the conversion of methanol, whereas the conversion of ethanol and 2-propanol decreases substantially to 26% and 9%, respectively, of those observed for the monolayer film of $Ti_{0.87}O_2$ nanosheets. The relatively small kinetic diameter of methanol (3.7 Å) enables its rapid diffusion through the MFI channels; consequently, methanol oxidation is not significantly hindered by diffusional limitations. However, as the kinetic diameter of the reactant approaches the dimensions of the MFI channels (4.4 Å for ethanol and 4.9 Å for 2-propanol; 5.1 Å × 5.5 Å and 5.3 Å × 5.6 Å for the MFI channels, respectively), diffusional limitations increasingly hinder molecular transport through the zeolite micropores, resulting in a pronounced suppression of the overall reaction rate. Moreover, the MFI overlayer appears to shift the product selectivity toward CO_2 for both 2-propanol and ethanol (Figure S12). The higher degree of oxidation may be attributed to the prolonged retention of reaction intermediates within the zeolite channels in close proximity to the photocatalytically active $Ti_{0.87}O_2$ nanosheets, thereby promoting their further oxidation to CO_2. This result also supports the conclusion that the alcohol molecules are transported through the micropores of MFI, making it unlikely that the decrease in reaction conversion is caused by the adsorption of the alcohol molecules onto the overlapping MFI nanosheets or the unexfoliated material observed in the AFM images. Additionally, the MFI zeolite is known to catalyze the dehydration of alcohols to ethers or alkenes; however, no evidence of such reaction pathways was observed. Only CO_2 and intermediates of the photo-oxidation reactions, such as acetone and acetaldehyde, were detected. The low partial pressure of the alcohols, the presence of water, and the low reaction temperature disfavor such side reactions.[69,70] These results demonstrate that the microporous MFI overlayer permits efficient photocatalytic oxidation of small molecules such as methanol, whereas the oxidation of bulkier molecules is substantially hindered by diffusional limitations. The bilayer architecture therefore influences both the product selectivity of photocatalytic oxidation and the accessibility of reactants by integrating the high oxidative activity of $Ti_{0.87}O_2$ nanosheets with the diffusion constraints imposed by the MFI zeolite overlayer. The extent to which reactants can access the photocatalytically active $Ti_{0.87}O_2$ surface depends on its kinetic diameter and intrinsic reactivity.

CONCLUSIONS

In this study, the photocatalytic oxidation of 2-propanol over titania nanosheets under UV irradiation was systematically examined, with particular emphasis on the effects of nanosheet morphology, supporting substrate, and interfacial design. The initial reaction rate increased with increasing lateral nanosheet size; however, nanosheets with lateral dimensions of 3−6 μm exhibited the highest long-term photocatalytic performance, indicating the presence of an optimal nanosheet size that balances charge separation efficiency and photocatalyst stability. The nature of the supporting substrate also exerted a pronounced influence on the photocatalytic behavior. In particular, variations in the reaction rate and product distribution reflected differences in charge carrier recombination arising from differences in substrate resistivity. Further enhancement of the photocatalytic performance was achieved through nanosheet sectioning, which resulted in a substantial increase in activity. This enhancement is attributed to the formation of nanosheet edges exposing well-defined crystallographic facets, in contrast to the randomly oriented edges generated during the exfoliation process. The intrinsic photocatalytic reactivity of the monolayer titania nanosheet film followed the order 2-propanol > ethanol > methanol, consistent with the relative stability of the intermediate radicals formed during the initial oxidation step. However, the deposition of a microporous MFI zeolite nanosheet overlayer substantially altered the conversion of these alcohols by imposing additional diffusional constraints. The conversion of larger alcohols was markedly suppressed, whereas the conversion of methanol remained essentially unchanged, indicating that the accessibility of the photocatalytically active titania surface is strongly influenced by the kinetic diameter of the reactant. These findings demonstrate that the photocatalytic properties of titania nanosheets can be rationally tailored through precise control of nanosheet size, morphology, and substrate characteristics, while the accessibility of reactants can be further modulated through integration with a microporous zeolitic overlayer. The present approach therefore provides a versatile platform for designing advanced photocatalytic systems that combine enhanced activity with tunable reactant accessibility, with potential applications in solar-driven chemical transformations and environmental remediation.

Downloaded from pubs.acs.org/aanm6/article-pdf/9/44/20956/6889460/an6c04766.pdf by NATL INST FOR MATLS SCIENCE (NIMS) user on 07 November 2026

https://doi.org/10.1021/acsanm.6c04766
ACS Appl. Nano Mater. 2026, 9, 20956–20966

■ ASSOCIATED CONTENT

Supporting Information

The Supporting Information is available free of charge at https://pubs.acs.org/doi/10.1021/acsanm.6c04766.

Characterization of precursor-layered materials of titanate and MFI zeolite; AFM and/or SEM images of monolayer films of titania nanosheets and zeolite nanosheets; in-plane XRD patterns of monolayer and bilayer films composed of titania and zeolite nanosheets; photocatalytic conversions of 2-propanol and yields of acetone and CO_2; schematic illustration of electronic band structure of titania nanosheets and substrates used; and characteristics of the substrates used and deposited films of titania nanosheets (PDF)

■ AUTHOR INFORMATION

Corresponding Author

Nobuyuki Sakai − *Research Center for Materials Nanoarchitectonics (MANA), National Institute for Materials Science (NIMS), Tsukuba, Ibaraki 305-0044, Japan;* orcid.org/0000-0002-9395-6751; Email: sakai.nobuyuki@nims.go.jp

Authors

Ondřej Veselý − *Research Center for Materials Nanoarchitectonics (MANA), National Institute for Materials Science (NIMS), Tsukuba, Ibaraki 305-0044, Japan;* orcid.org/0000-0002-8350-7725

Takayoshi Sasaki − *Research Center for Materials Nanoarchitectonics (MANA), National Institute for Materials Science (NIMS), Tsukuba, Ibaraki 305-0044, Japan;* orcid.org/0000-0002-2872-0427

Complete contact information is available at: https://pubs.acs.org/doi/10.1021/acsanm.6c04766

Author Contributions

O.V.—investigation, formal analysis, and writing—original draft; N.S.—methodology and writing—review and editing; T.S.—conceptualization and writing—review and editing.

Notes

The authors declare no competing financial interest.

■ ACKNOWLEDGMENTS

This work was supported by the World Premier International Research Center Initiative (WPI), Ministry of Education, Culture, Sports, Science and Technology (MEXT), Japan, and the CREST of the Japan Science and Technology Agency (JST) (grant no. JPMJCR22B1), Japan. The in-plane XRD measurements were performed under the approval of the Photon Factory Program Advisory Committee (Proposal No. 2024G501). O.V. acknowledges Dr. Takayuki Kikuchi for providing the suspension of the large titania nanosheets.

■ REFERENCES

(1) Li, Z.; Wang, S.; Wu, J.; Zhou, W. Recent Progress in Defective TiO_2 Photocatalysts for Energy and Environmental Applications. *Renewable Sustainable Energy Rev.* **2022**, *156*, 111980.

(2) Van Thuan, D.; Ngo, H. L.; Thi, H. P.; Chu, T. T. H. Photodegradation of Hazardous Organic Pollutants Using Titanium Oxides -Based Photocatalytic: A Review. *Environ. Res.* **2023**, *229*, 116000.

(3) Sari, Y.; Gareso, P. L.; Armynah, B.; Tahir, D. A Review of TiO_2 Photocatalyst for Organic Degradation and Sustainable Hydrogen Energy Production. *Int. J. Hydrogen Energy* **2024**, *55*, 984−996.

(4) Guo, Q.; Zhou, C.; Ma, Z.; Yang, X. Fundamentals of TiO_2 Photocatalysis: Concepts, Mechanisms, and Challenges. *Adv. Mater.* **2019**, *31*, 1901997.

(5) Yamakata, A.; Vequizo, J. J. M. Curious Behaviors of Photogenerated Electrons and Holes at the Defects on Anatase, Rutile, and Brookite TiO_2 Powders: A Review. *J. Photochem. Photobiol., C* **2019**, *40*, 234−243.

(6) Shayegan, Z.; Lee, C.-S.; Haghighat, F. TiO_2 Photocatalyst for Removal of Volatile Organic Compounds in Gas Phase—A Review. *Chem. Eng. J.* **2018**, *334*, 2408−2439.

(7) Weon, S.; He, F.; Choi, W. Status and Challenges in Photocatalytic Nanotechnology for Cleaning Air Polluted with Volatile Organic Compounds: Visible Light Utilization and Catalyst Deactivation. *Environ. Sci.:Nano* **2019**, *6*, 3185−3214.

(8) Allen, M. R.; Thibert, A.; Sabio, E. M.; Browning, N. D.; Larsen, D. S.; Osterloh, F. E. Evolution of Physical and Photocatalytic Properties in the Layered Titanates $A_2Ti_4O_9$ (A = K, H) and in Nanosheets Derived by Chemical Exfoliation. *Chem. Mater.* **2010**, *22*, 1220−1228.

(9) Dong, X.; Cheng, F. Recent Development in Exfoliated Two-Dimensional g-C_3N_4 Nanosheets for Photocatalytic Applications. *J. Mater. Chem. A* **2015**, *3*, 23642−23652.

(10) Yuan, Y.-J.; Shen, Z.; Wu, S.; Su, Y.; Pei, L.; Ji, Z.; Ding, M.; Bai, W.; Chen, Y.; Yu, Z.-T.; Zou, Z. Liquid Exfoliation of g-C_3N_4 Nanosheets to Construct 2D-2D MoS_2/g-C_3N_4 Photocatalyst for Enhanced Photocatalytic H_2 Production Activity. *Appl. Catal., B* **2019**, *246*, 120−128.

(11) Sakai, N.; Ebina, Y.; Takada, K.; Sasaki, T. Electronic Band Structure of Titania Semiconductor Nanosheets Revealed by Electrochemical and Photoelectrochemical Studies. *J. Am. Chem. Soc.* **2004**, *126*, 5851−5858.

(12) Zhou, W.; Umezawa, N.; Ma, R.; Sakai, N.; Ebina, Y.; Sano, K.; Liu, M.; Ishida, Y.; Aida, T.; Sasaki, T. Spontaneous Direct Band Gap, High Hole Mobility, and Huge Exciton Energy in Atomic-Thin TiO_2 Nanosheet. *Chem. Mater.* **2018**, *30*, 6449−6457.

(13) Shibata, T.; Takanashi, G.; Nakamura, T.; Fukuda, K.; Ebina, Y.; Sasaki, T. Titanoniobate and Niobate Nanosheet Photocatalysts: Superior Photoinduced Hydrophilicity and Enhanced Thermal Stability of Unilamellar Nb_3O_8 Nanosheet. *Energy Environ. Sci.* **2011**, *4*, 535−542.

(14) Jung, H.; Cha, G.; Kim, H.; Will, J.; Zhou, X.; Spiecker, E.; Breu, J.; Schmuki, P. Ultrathin Ti-Deficient TiO_2 Nanosheets with Pt Single Atoms Enable Efficient Photocatalytic Nitrate Reduction to Ammonia. *J. Am. Chem. Soc.* **2025**, *147*, 9049−9055.

(15) Tae, E. L.; Lee, K. E.; Jeong, J. S.; Yoon, K. B. Synthesis of Diamond-Shape Titanate Molecular Sheets with Different Sizes and Realization of Quantum Confinement Effect during Dimensionality Reduction from Two to Zero. *J. Am. Chem. Soc.* **2008**, *130*, 6534−6543.

(16) Katal, R.; Masudy-Panah, S.; Tanhaei, M.; Farahani, M. H. D. A.; Jiangyong, H. A Review on the Synthesis of the Various Types of Anatase TiO_2 Facets and Their Applications for Photocatalysis. *Chem. Eng. J.* **2020**, *384*, 123384.

(17) Timmerman, M. A.; Xia, R.; Le, P. T. P.; Wang, Y.; ten Elshof, J. E. Metal Oxide Nanosheets as 2D Building Blocks for the Design of Novel Materials. *Chem. - Eur. J.* **2020**, *26*, 9084−9098.

(18) Shibata, T.; Sakai, N.; Fukuda, K.; Ebina, Y.; Sasaki, T. Photocatalytic Properties of Titania Nanostructured Films Fabricated from Titania Nanosheets. *Phys. Chem. Chem. Phys.* **2007**, *9*, 2413−2420.

(19) Sakai, N.; Kamanaka, K.; Sasaki, T. Modulation of Photochemical Activity of Titania Nanosheets via Heteroassembly with Reduced Graphene Oxide. Enhancement of Photoinduced Hydrophilic Conversion Properties. *J. Phys. Chem. C* **2016**, *120*, 23944−23950.

Downloaded from pubs.acs.org/aanmf6/article-pdf/9/44/20956/6889460/an6c04766.pdf by NATL INST FOR MATLS SCIENCE (NIMS) user on 07 November 2026

(20) Cai, X.; Ozawa, T. C.; Funatsu, A.; Ma, R.; Ebina, Y.; Sasaki, T. Tuning the Surface Charge of 2D Oxide Nanosheets and the Bulk-Scale Production of Superlatticelike Composites. *J. Am. Chem. Soc.* **2015**, *137*, 2844−2847.
(21) Sakai, N.; Fukuda, K.; Omomo, Y.; Ebina, Y.; Takada, K.; Sasaki, T. Hetero-nanostructured Films of Titanium and Manganese Oxide Nanosheets: Photoinduced Charge Transfer and Electrochemical Properties. *J. Phys. Chem. C* **2008**, *112*, 5197−5202.
(22) Lotsch, B. V. Vertical 2D Heterostructures. *Annu. Rev. Mater. Res.* **2015**, *45*, 85−109.
(23) Sakai, N.; Sasaki, T. Highly Organized Monolayer Arrangement of 2D Materials and Its Applications. *Acc. Mater. Res.* **2024**, *5*, 752−760.
(24) Sasaki, T.; Ebina, Y.; Fukuda, K.; Tanaka, T.; Harada, M.; Watanabe, M. Titania Nanostructured Films Derived from a Titania Nanosheet/Polycation Multilayer Assembly via Heat Treatment and UV Irradiation. *Chem. Mater.* **2002**, *14*, 3524−3530.
(25) Smit, B.; Maesen, T. L. M. Towards a Molecular Understanding of Shape Selectivity. *Nature* **2008**, *451*, 671−678.
(26) Smit, B.; Maesen, T. L. M. Molecular Simulations of Zeolites: Adsorption, Diffusion, and Shape Selectivity. *Chem. Rev.* **2008**, *108*, 4125−4184.
(27) Guo, J.; Qin, Y.; Zhu, Y.; Zhang, X.; Long, C.; Zhao, M.; Tang, Z. Metal−Organic Frameworks as Catalytic Selectivity Regulators for Organic Transformations. *Chem. Soc. Rev.* **2021**, *50*, 5366−5396.
(28) Canlas, C. P.; Lu, J.; Ray, N. A.; Grosso-Giordano, N. A.; Lee, S.; Elam, J. W.; Winans, R. E.; Van Duyne, R. P.; Stair, P. C.; Notestein, J. M. Shape-Selective Sieving Layers on an Oxide Catalyst Surface. *Nat. Chem.* **2012**, *4*, 1030−1036.
(29) Csicsery, S. M. Shape-Selective Catalysis in Zeolites. *Zeolites* **1984**, *4*, 202−213.
(30) Roth, W. J.; Nachtigall, P.; Morris, R. E.; Čejka, J. Two-Dimensional Zeolites: Current Status and Perspectives. *Chem. Rev.* **2014**, *114*, 4807−4837.
(31) Roth, W. J.; Opanasenko, M.; Mazur, M.; Gil, B.; Čejka, J.; Sasaki, T. Current State and Perspectives of Exfoliated Zeolites. *Adv. Mater.* **2024**, *36*, 2307341.
(32) Roth, W. J.; Sasaki, T.; Wolski, K.; Gil, B.; Zapotoczny, S.; Čejka, J.; Kubů, M.; Mazur, M.; Ebina, Y.; Sakai, N.; Tang, D.-M.; Ma, R. Exfoliating Layered Zeolite MFI into Unilamellar Nanosheets in Solution as Precursors for the Synthesis of Hierarchical Nanocomposites and Oriented Films. *Inorg. Chem. Front.* **2023**, *10*, 1511−1521.
(33) Sabnis, S.; Tanna, V. A.; Li, C.; Zhu, J.; Vattipalli, V.; Nonnenmann, S. S.; Sheng, G.; Lai, Z.; Winter, H. H.; Fan, W. Exfoliation of Two-Dimensional Zeolites in Liquid Polybutadienes. *Chem. Commun.* **2017**, *53*, 7011−7014.
(34) Maheshwari, S.; Jordan, E.; Kumar, S.; Bates, F. S.; Penn, R. L.; Shantz, D. F.; Tsapatsis, M. Layer Structure Preservation during Swelling, Pillaring, and Exfoliation of a Zeolite Precursor. *J. Am. Chem. Soc.* **2008**, *130*, 1507−1516.
(35) Wang, L.; Dong, F.; Meng, Y.; Kang, Y.; Zhang, H.; Tang, Z. Molecular Sieve Confined Catalysts for the Catalytic Combustion of VOCs: Preparation, Application and Future Development. *J. Mater. Chem. A* **2025**, *13*, 18209−18252.
(36) Kovalevskiy, N. S.; Lyulyukin, M. N.; Selishchev, D. S.; Kozlov, D. V. Analysis of Air Photocatalytic Purification Using a Total Hazard Index: Effect of the Composite TiO_2/Zeolite Photocatalyst. *J. Hazard. Mater.* **2018**, *358*, 302−309.
(37) Sasaki, T.; Watanabe, M. Osmotic Swelling to Exfoliation. Exceptionally High Degrees of Hydration of a Layered Titanate. *J. Am. Chem. Soc.* **1998**, *120*, 4682−4689.
(38) Sasaki, T.; Kooli, F.; Iida, M.; Michiue, Y.; Takenouchi, S.; Yajima, Y.; Izumi, F.; Chakoumakos, B. C.; Watanabe, M. A Mixed Alkali Metal Titanate with the Lepidocrocite-like Layered Structure. Preparation, Crystal Structure, Protonic Form, and Acid−Base Intercalation Properties. *Chem. Mater.* **1998**, *10*, 4123−4128.
(39) Maluangnont, T.; Matsuba, K.; Geng, F.; Ma, R.; Yamauchi, Y.; Sasaki, T. Osmotic Swelling of Layered Compounds as a Route to Producing High-Quality Two-Dimensional Materials. A Comparative Study of Tetramethylammonium versus Tetrabutylammonium Cation in a Lepidocrocite-Type Titanate. *Chem. Mater.* **2013**, *25*, 3137−3146.
(40) Sakai, N.; Suzuki, M.; Sasaki, T. Scission of 2D Inorganic Nanosheets via Physical Adsorption on a Nonflat Surface. *Adv. Mater. Interfaces* **2022**, *9*, 2102591.
(41) Tanaka, T.; Ebina, Y.; Takada, K.; Kurashima, K.; Sasaki, T. Oversized Titania Nanosheet Crystallites Derived from Flux-Grown Layered Titanate Single Crystals. *Chem. Mater.* **2003**, *15*, 3564−3568.
(42) Geng, F.; Ma, R.; Ebina, Y.; Yamauchi, Y.; Miyamoto, N.; Sasaki, T. Gigantic Swelling of Inorganic Layered Materials: A Bridge to Molecularly Thin Two-Dimensional Nanosheets. *J. Am. Chem. Soc.* **2014**, *136*, 5491−5500.
(43) Song, Y.; Sakai, N.; Ebina, Y.; Iyi, N.; Kikuchi, T.; Ma, R.; Ishida, Y.; Sasaki, T. Systematic Study on Swelling/Delamination of Layered Metal Oxides with Quaternary Ammonium Ions: Production of Well-Shaped/Oversized Unilamellar Nanosheets. *Small Methods* **2025**, *9*, 2401055.
(44) Choi, M.; Na, K.; Kim, J.; Sakamoto, Y.; Terasaki, O.; Ryoo, R. Stable Single-Unit-Cell Nanosheets of Zeolite MFI as Active and Long-Lived Catalysts. *Nature* **2009**, *461*, 246−249.
(45) Na, K.; Park, W.; Seo, Y.; Ryoo, R. Disordered Assembly of MFI Zeolite Nanosheets with a Large Volume of Intersheet Mesopores. *Chem. Mater.* **2011**, *23*, 1273−1279.
(46) Park, W.; Yu, D.; Na, K.; Jelfs, K. E.; Slater, B.; Sakamoto, Y.; Ryoo, R. Hierarchically Structure-Directing Effect of Multi-Ammonium Surfactants for the Generation of MFI Zeolite Nanosheets. *Chem. Mater.* **2011**, *23*, 5131−5137.
(47) Sakai, N.; Sasaki, T. Guidelines for Arranging 2D Nanosheets into Neatly Tiled Monolayer Films by a Spin-Coating Process. *Langmuir* **2022**, *38*, 12399−12407.
(48) Chang, C.-P.; Chen, J.-N.; Lu, M.-C. Characteristics of Photocatalytic Oxidation of Gaseous 2-Propanol Using Thin-Film TiO_2 Photocatalyst. *J. Chem. Technol. Biotechnol.* **2004**, *79*, 1293−1300.
(49) Arsac, F.; Bianchi, D.; Chovelon, J. M.; Ferronato, C.; Herrmann, J. M. Experimental Microkinetic Approach of the Photocatalytic Oxidation of Isopropyl Alcohol on TiO_2. Part 2. From the Surface Elementary Steps to the Rates of Oxidation of the C_3H_xO Species. *J. Phys. Chem. A* **2006**, *110*, 4213−4222.
(50) Muñoz-Batista, M. J.; Ballari, M. M.; Kubacka, A.; Alfano, O. M.; Fernández-García, M. Braiding Kinetics and Spectroscopy in Photo-Catalysis: The Spectro-Kinetic Approach. *Chem. Soc. Rev.* **2019**, *48*, 637−682.
(51) Wu, S.; Ishisone, K.; Sheng, Y.; Manuputty, M. Y.; Kraft, M.; Xu, R. TiO_2 with Controllable Oxygen Vacancies for Efficient Isopropanol Degradation: Photoactivity and Reaction Mechanism. *Catal. Sci. Technol.* **2021**, *11*, 4060−4071.
(52) Matsumoto, Y.; Ida, S.; Inoue, T. Photodeposition of Metal and Metal Oxide at the TiO_x Nanosheet to Observe the Photocatalytic Active Site. *J. Phys. Chem. C* **2008**, *112*, 11614−11616.
(53) Carroll, E. C.; Compton, O. C.; Madsen, D.; Osterloh, F. E.; Larsen, D. S. Ultrafast Carrier Dynamics in Exfoliated and Functionalized Calcium Niobate Nanosheets in Water and Methanol. *J. Phys. Chem. C* **2008**, *112*, 2394−2403.
(54) Sannino, D.; Vaiano, V.; Ciambelli, P.; Eloy, P.; Gaigneaux, E. M. Avoiding the Deactivation of Sulphated MoO_x/TiO_2 Catalysts in the Photocatalytic Cyclohexane Oxidative Dehydrogenation by a Fluidized Bed Photoreactor. *Appl. Catal., A* **2011**, *394*, 71−78.
(55) Pylnev, M.; Wong, M.-S. Comparative Study of Photocatalytic Deactivation of Pure and Black Titania Thin Films. *J. Photochem. Photobiol., A* **2019**, *378*, 125−130.
(56) Liu, T.; Zhang, X.; Zhang, J.; Wang, W.; Feng, L.; Wu, L.; Li, W.; Zeng, G.; Li, B. Interface Study of ITO/ZnO and ITO/SnO_2 Complex Transparent Conductive Layers and Their Effect on CdTe Solar Cells. *Int. J. Photoenergy* **2013**, *2013*, 765938.
(57) Fujimura, N.; Ohta, A.; Makihara, K.; Miyazaki, S. Evaluation of Valence Band Top and Electron Affinity of SiO_2 and Si-Based Semiconductors Using X-Ray Photoelectron Spectroscopy. *Jpn. J. Appl. Phys.* **2016**, *55*, 08PC06.

Downloaded from pubs.acs.org/aanm6/article-pdf/9/44/20956/6889460/an6c04766.pdf by NATL INST FOR MATLS SCIENCE (NIMS) user on 07 November 2026

https://doi.org/10.1021/acsanm.6c04766
ACS Appl. Nano Mater. 2026, 9, 20956−20966

(58) Wang, Y.; Tang, W. Surface-Dependent Conductivity, Transition Type, and Energy Band Structure in Amorphous Indium Tin Oxide Films. *Solid-State Electron.* **2017**, *138*, 79−83.
(59) Osuagwu, B.; Raza, W.; Tesler, A. B.; Schmuki, P. A Drastic Improvement in Photocatalytic H_2 Production by TiO_2 Nanosheets Grown Directly on Ta_2O_5 Substrates. *Nanoscale* **2021**, *13*, 12750−12756.
(60) Lu, Y.; Wang, G.; Zhang, H.; Zhang, Y.; Kang, S.; Zhao, H. Photoelectrochemical Manifestation of Intrinsic Photoelectron Transport Properties of Vertically Aligned {001} Faceted Single Crystal TiO_2 Nanosheet Films. *RSC Adv.* **2015**, *5*, 55438−55444.
(61) Shiraishi, Y.; Shiota, S.; Hirakawa, H.; Tanaka, S.; Ichikawa, S.; Hirai, T. Titanium Dioxide/Reduced Graphene Oxide Hybrid Photocatalysts for Efficient and Selective Partial Oxidation of Cyclohexane. *ACS Catal.* **2017**, *7*, 293−300.
(62) Ciriminna, R.; Parrino, F.; De Pasquale, C.; Palmisano, L.; Pagliaro, M. Photocatalytic Partial Oxidation of Limonene to 1,2 Limonene Oxide. *Chem. Commun.* **2018**, *54*, 1008−1011.
(63) Liu, L.; Gu, X.; Ji, Z.; Zou, W.; Tang, C.; Gao, F.; Dong, L. Anion-Assisted Synthesis of TiO_2 Nanocrystals with Tunable Crystal Forms and Crystal Facets and Their Photocatalytic Redox Activities in Organic Reactions. *J. Phys. Chem. C* **2013**, *117*, 18578−18587.
(64) Kim, J.; Schmuki, P. Facet-Dependent Photocatalytic Activity of Rutile and Anatase Single Crystals in the Presence and Absence of a Pt Cocatalyst. *ACS Catal.* **2025**, *15*, 12790−12799.
(65) Jung, H.; Cha, G.; Kim, H.; Will, J.; Zhou, X.; Bad'ura, Z.; Zoppellaro, G.; Dobrota, A. S.; Skorodumova, N. V.; Pašti, I. A.; Sarma, B. B.; Schmidt, J.; Spiecker, E.; Breu, J.; Schmuki, P. Cation Vacancies in Ti-Deficient TiO_2 Nanosheets Enable Highly Stable Trapping of Pt Single Atoms for Persistent Photocatalytic Hydrogen Evolution. *Small* **2025**, *21*, 2502428.
(66) Yamagata, S.; Nakabayashi, S.; Sancier, K. M.; Fujishima, A. Photocatalytic Oxidation of Alcohols on TiO_2. *Bull. Chem. Soc. Jpn.* **1988**, *61*, 3429−3434.
(67) Hatipoğlu, A.; Çinar, Z. A QSAR Study on the Kinetics of the Reactions of Aliphatic Alcohols with the Photogenerated Hydroxyl Radicals. *J. Mol. Struct. THEOCHEM* **2003**, *631*, 189−207.
(68) Yurdakal, S.; Augugliaro, V. Partial Oxidation of Aromatic Alcohols via TiO_2 Photocatalysis: The Influence of Substituent Groups on the Activity and Selectivity. *RSC Adv.* **2012**, *2*, 8375−8380.
(69) Zhi, Y.; Shi, H.; Mu, L.; Liu, Y.; Mei, D.; Camaioni, D. M.; Lercher, J. A. Dehydration Pathways of 1-Propanol on HZSM-5 in the Presence and Absence of Water. *J. Am. Chem. Soc.* **2015**, *137*, 15781−15794.
(70) Lepore, A. W.; Li, Z.; Davison, B. H.; Foo, G.-S.; Wu, Z.; Narula, C. K. Catalytic Dehydration of Biomass Derived 1-Propanol to Propene over M-ZSM-5 (M = H, V, Cu, or Zn). *Ind. Eng. Chem. Res.* **2017**, *56*, 4302−4308.

Downloaded from pubs.acs.org/aanm6/article-pdf/9/44/20956/6889546O/an6c04766.pdf by NATL INST FOR MATLS SCIENCE (NIMS) user on 07 November 2026

https://doi.org/10.1021/acsanm.6c04766
ACS Appl. Nano Mater. 2026, 9, 20956−20966